Defect-Assisted Exciton Transfer across the Tetracene-Si(111):H Interface

Marvin Krenz, Uwe Gerstmann, and Wolf Gero Schmidt
Lehrstuhl für Theoretische Materialphysik, Universität Paderborn, 33095 Paderborn, Germany

(Received 15 June 2023; accepted 23 January 2024; published 16 February 2024)

Exciton transfers are ubiquitous and extremely important processes, but often poorly understood. A recent example is the triplet exciton transfer in tetracene sensitized silicon solar cells exploited for harvesting high-energy photons. The present *ab initio* molecular dynamics calculations for tetracene-Si(111):H interfaces show that Si dangling bonds, intuitively expected to hinder the exciton transfer, actually foster it. This suggests that defects and structural imperfections at interfaces may be exploited for excitation transfer.

DOI: 10.1103/PhysRevLett.132.076201

The transfer of excitons, i.e., bound electron-hole pairs, is highly relevant for numerous physical, chemical, and biological processes. The energy transport in photosynthetic organisms [1], efficient solid-state lighting [2], or the harvesting of light by organic solar cells [3,4] are prominent examples. Accordingly, there is much interest in the details of the transfer mechanism [5–9]. Recently, the exciton transfer across the organic-inorganic interface of singlet fission-sensitized silicon solar cells, shown schematically in Fig. 1, has received much attention [10–13].

Singlet fission, i.e., the down-conversion of singlet excitons into pairs of triplet excitons in a sensitizing layer, has the potential to generate additional photocurrent from photons with energies larger than the band gap [14,15]. This promises to break the Shockley-Queisser limit for solar cell efficiencies [16,17]. Tetracene (Tc) is an archetypical material for singlet fission [18] and has been used successfully to sensitize Si solar cells [10,11]. However, the mechanism by which the triplet excitons are efficiently transferred across the tetracene-silicon interface is not understood [10–13,19]. Einzinger *et al.* [10] suggested electric-field-effect passivation at the interface. In contrast, a more recent work by the Ehrler group [19] proposes covalent bonding between the sensitizing layer and the Si surface for transfer optimization.

These suggestions are challenged by the *ab initio* molecular dynamics (AIMD) calculations presented in this Letter. Our study focusses on the Tc-Si(111):H interface and demonstrates that in particular Si dangling bond defects play a key role for the exciton transfer. Interface defects are often considered detrimental to material performance, because they accelerate charge and energy losses [20]. In this case, however, they turn out to be instrumental for the excitation transfer.

Here spin-polarized density-functional theory (DFT) calculations are performed using the QUANTUM ESPRESSO package [21,22] with norm-conserving pseudopotentials. The Perdew-Burke-Ernzerhof (PBE) functional [23] within the generalized-gradient approximation is used to describe the electron exchange and correlation effects. Dispersion interactions are taken into account using Grimme's DFT-D2 approach [24]. In addition, hybrid DFT calculations are performed using the Heyd-Scuseria-Ernzerhof (HSE) functional [25]. Excited-state potential-energy surfaces (PES) obtained from constrained DFT [26–29] are used for AIMD calculations that describe the time evolution of the excitation [30,31]. Libra-X package modules [32] and the Berendsen thermostat [33] are used to account for nonadiabatic and temperature effects, respectively. Further details can be found in the Appendix.

The morphology of the interface between Tc and the Si(111):H surface depends on the preparation conditions. Tc thin films grown below temperatures of 265 K are dominated by almost upright-standing molecules forming a high-density (HD) phase, the so-called Tc II phase [34].

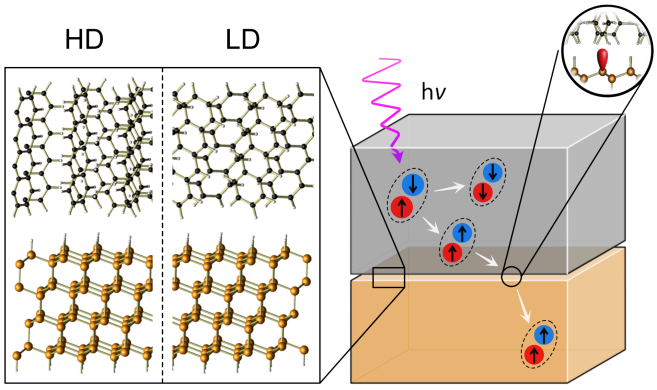

FIG. 1. Scheme showing part of a singlet fission-sensitized silicon solar cell. Absorption of a high-energy photon by the tetracene layer produces a singlet exciton. This singlet exciton undergoes singlet fission to generate two triplet excitons. These excitons are then transferred into the Si solar cell. Enlarged image details (left) show side views of the models used for the interface between Si(111):H and high-density (HD) as well as low-density (LD) Tc phases. Also shown is an interface dangling bond defect (right).

 © 2024 American Physical Society

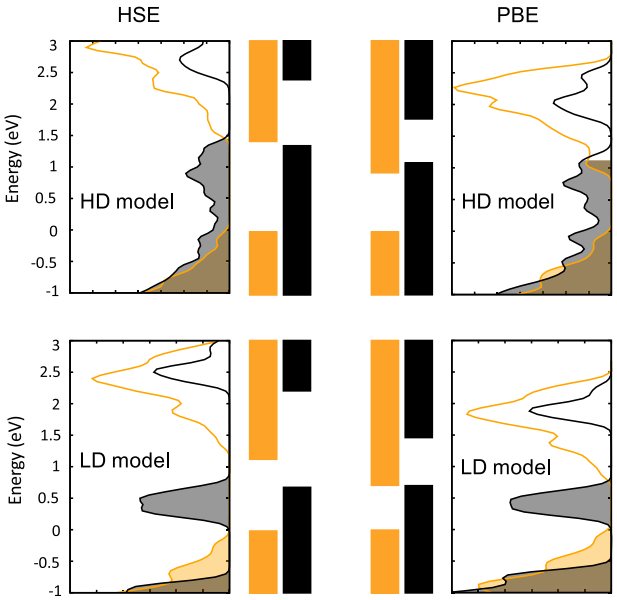

FIG. 2. Density of states and band alignment for Tc overlayers on Si(111):H calculated on the HSE and PBE levels of theory. Energies refer to the Si valence band maximum (VBM). Black and orange denote Tc- and Si-related states, respectively. Occupied states are shaded.

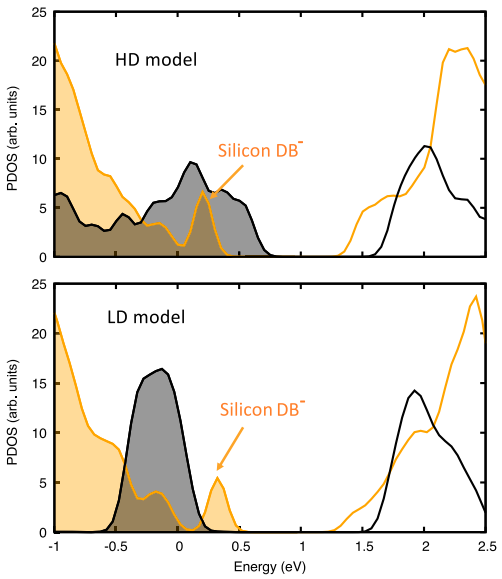

FIG. 3. Partial density of states (PDOS) for Tc overlayers on defective $\mathrm{Si(111):H + DB^-}$ calculated on the HSE level of theory. Energies refer to the Si VBM. Black and orange denote Tc- and Si-related states. Occupied states are shaded.

Annealing results in a low-density (LD) phase of tilted molecules, similar to the Tc I bulk phase. The respective interfaces are modeled here with the HD and LD monolayer structures sketched in Fig. 1. These models (see Ref. [35] for atomic coordinates) have been shown to be consistent with near-edge x-ray absorption fine structure data [34]. They have a 5×5 and 11×4 lateral periodicity and are characterized by a minimum molecule-molecule distance of 3.32 and 3.51 Å, respectively. The supercells contain 8 atomic Si layers, an overlayer consisting of 8 molecules, and a vacuum region of 10 Å.

In Fig. 2 the calculated band alignment at the Tc-Si(111):H interface can be seen. Within HSE, a type-II, i.e., staggered band alignment, is obtained for both the LD and HD models. This agrees with earlier hybrid DFT results [36] and suggests the possibility of exciton dissociation at the interface with electron transfer to Si. We probed that possibility by performing room temperature AIMD calculations, using a Tc-localized T_1 triplet exciton as start configuration. However, at ideal interfaces, neither exciton nor charge transfer occurs.

Real interfaces are characterized by defects, which profoundly influence their electronic properties [37]. In case of hydrogenated Si interfaces, the appearance of Si dangling bonds (DB) due to missing hydrogen can be expected [38–41] and is considered in the following. In case of *n*-type Si(111) as used experimentally [12,34], the DB state is doubly occupied in the ground state. The calculated densities of states for the HD and LD interface models with DB defect (see Ref. [35] for atomic coordinates) are shown in Fig. 3. The Si $\mathrm{DB^-}$ state appears about 0.2 eV above the Si valence band maximum (VBM). While its energy is within the occupied Tc states of the HD phase, it is above the corresponding Tc states of the LD phase. This results from the lower molecular density at the LD interface, which leads to weaker dispersion of the molecular states.

Do the DB states alter the conditions for exciton transfer? In case of the LD phase, this is suggested by the effective type-I band alignment at the defective interface; see Fig. 3. It allows for an energetically favorable transfer of both holes and excited electrons from Tc to Si. In fact, room temperature AIMD results in an immediate exciton transfer from Tc to Si. We mention that the measurements in Ref. [12] indicate indeed a type-I band alignment, in contrast to calculations for ideal interfaces [36].

The situation is different at the HD interface. Here the Si DB is lower in energy than the Tc valence band edge; see Fig. 3. Nevertheless, thermal activation results in an exciton transfer also in this case, as shown by room temperature AIMD. An example trajectory is shown in Fig. 4. At first, the exciton delocalizes within the Tc layer. After about 310 fs, the exciton hole is transferred to the Si DB. The resulting charge transfer state is short-lived. The electron follows the hole and completes the exciton transfer across the interface at about 330 fs. Now, both excited hole and electron are available in the Si substrate for extraction to the electrical contacts. The extraction will be easier for the immediately delocalized electron, compared to the hole that remains attracted to the DB defect.

We mention that not all charge transfer states lead to exciton transfer. In some instances, the DB localized hole

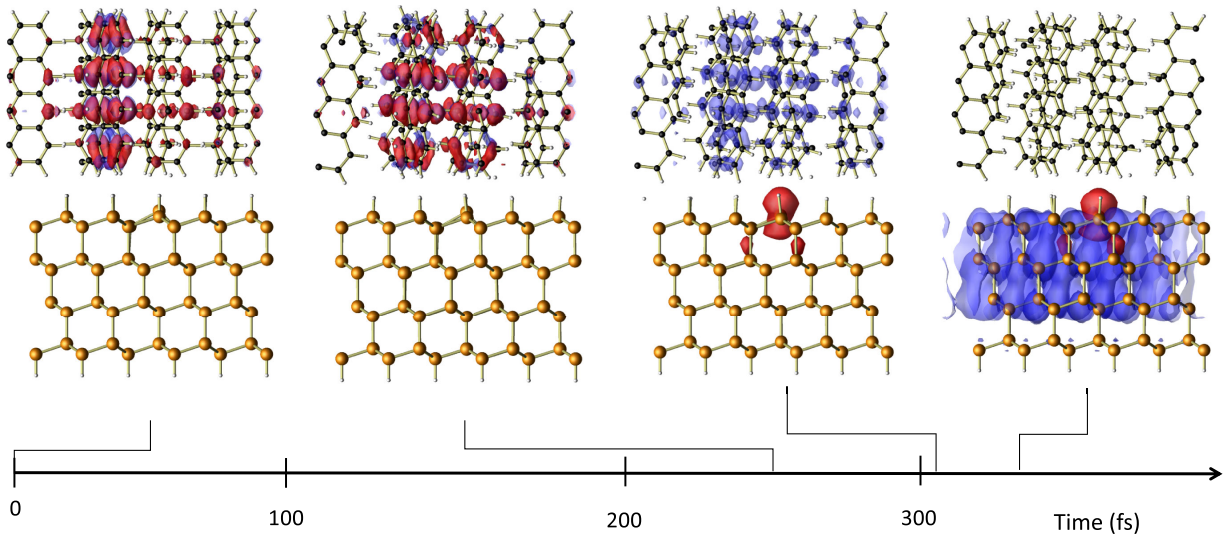

FIG. 4. Calculated room temperature dynamics of the exciton transfer at the Tc-Si(111):H interface (HD model with DB defect, example trajectory with characteristic snapshots at 0, 250, 310, and 330 fs after the exciton has been trapped in the lowest molecular layer). Blue and red isosurfaces indicate electron and hole localization, respectively.

returns temporarily to the Tc layer. However, all exciton transfer processes observed in the AIMD follow the scenario shown in Fig. 4, i.e., hole transfer precedes electron transfer. The timescales calculated here are comparable to the singlet exciton splitting times observed for hybrid junction solar cells [9].

By which mechanism does the Si surface DB enable the exciton transfer? In the 0 K ground-state configuration, the DB^- gives rise to a twofold occupied state slightly above the Si bulk VBM (see Fig. 3, top), but still below the Tc VB edge. However, at room temperature, the Si atom hosting the defect vibrates; i.e., it oscillates along the surface normal. This vibration is accompanied by a partial rehybridization, $sp^3 \leftrightarrow sp^2 + p$, and a corresponding variation of the DB energy [42]; see Fig. 5. In particular, the DB^- state assumes temporarily energies above the Tc VB edge. This fosters the hole transfer from the Tc film to silicon. The electron follows the hole with a delay of only a few femtoseconds and completes the exciton transfer. The transfer mechanism identified here is reminiscent of earlier findings for organic donor-acceptor blends, where molecular vibrations in concert with electronic transitions lead to rapid charge guiding [7].

How does temperature influence the exciton transfer? The rareness of transfer events in conjunction with the numerical expense of the excited-state AIMD does not allow for a direct calculation of converged transfer rates. In order to get some insight, AIMD is performed under the assumption that electron hopping occurs whenever it

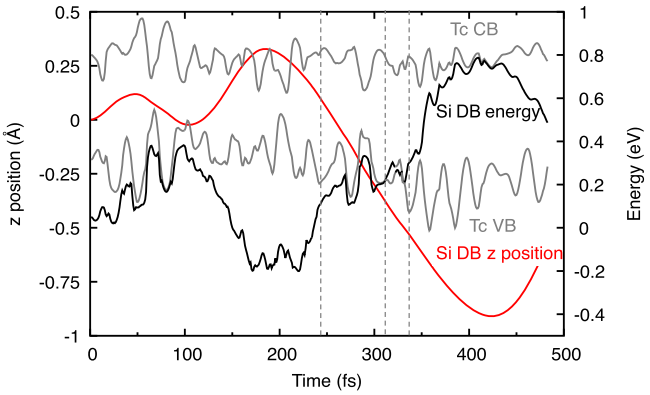

FIG. 5. Evolution of Tc valence band (VB) and conduction band (CB) edge as well as Si DB state energies along the AIMD trajectory shown in Fig. 4 (dashed vertical lines refer to the snapshots). Also shown is the z position of the Si DB surface atom (displacement along the surface normal).

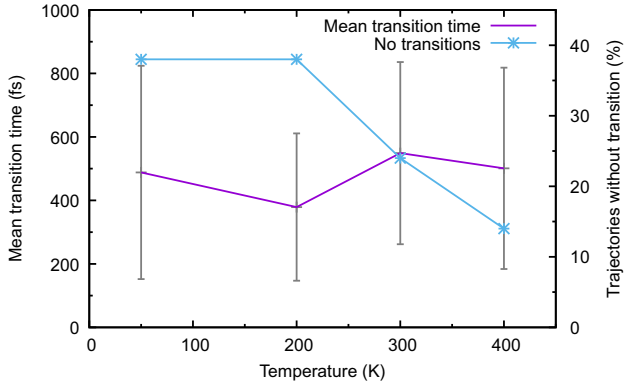

FIG. 6. Calculated average times (with standard deviation, assuming a 100% hopping probability) required for exciton transfer across the defective Tc-Si(111):H interface (HD model) in dependence on the simulation temperature. The number of trajectories (out of 50 in total) which did not lead to exciton transfer within 1 ps is also shown.

lowers the energy. Assuming thus a 100% hopping probability—in contrast to the calculated values that scatter between about 5% and 80%—the average transfer times shown in Fig. 6 are obtained. Values that broadly scatter around 500 fs are calculated, nearly independent of the temperature. This can be explained by the Si DB shuttling mechanism explained above. The $sp^3 \leftrightarrow sp^2 + p$ hybridization change is coupled to a very soft Si surface atom vibration at about 2.5 THz, which is activated already at low temperature. However, the exciton transfer time depends also on the phase relation between the vibrations in the Tc layer and the Si surface. This causes the large scatter of the calculated values. With low activation energy, i.e., for temperatures below 200 K, numerous trajectories do not lead to exciton transfer within the simulation time. Increasing temperature increases the chance to observe exciton transfer.

In summary, the present calculations demonstrate that exciton transfer across Tc-Si(111):H interfaces depends strongly on the interface morphology. Interestingly, common dangling bond defects at the interface improve rather than deteriorate the exciton transfer properties: Si dangling bonds give rise to interface states energetically close to the Tc valence band edge. They assist the hole transfer into Si bulk either directly—for low-density Tc layers—or upon thermal activation, in case of high-density Tc layers. The exciton electron follows the hole within a few femtoseconds. Since the number of DB defects depends sensitively on the operation conditions [43,44], more robust defects may need to be exploited in actual devices. In any case, the present calculations show that interface electronic states close to the band edges that temporally change in energy, e.g., due to vibrations, assist the charge shuttling and suggest that heterostructure imperfections, e.g., defects or inhomogeneities in density and layer thickness, can be utilized for the optimization of the charge and excitation transfer properties of nanomaterials.

The DFG (TRR 142/3-2023—Project No. 231447078 and SCHM1361/33) is gratefully acknowledged for financial support. We thank the Paderborn Center for Parallel Computing (PC^2) and the Höchstleistungs-Rechenzentrum Stuttgart (HLRS) for grants of high-performance computer time.

Appendix: Computational details.—Table I compares measured data for Si and Tc excitation energies with DFT calculations using PBE as well as HSE (with 25% and 40% exact exchange), and B3LYP [45]. HSE provides roughly correct values for both Tc and Si, while HSE40 and B3LYP overestimate the Si band gap. PBE underestimates the Si band gap. Excited-state PES calculated within PBE and HSE are shown in Fig. 7. Here the energies of both Tc and Si localized excitons are studied in dependence on the Si dangling bond position. Both within PBE and HSE, Tc- and Si-localized excitons correspond to local and global energy minima, respectively. The intersection of the corresponding PES occurs at slightly different geometries, and the transition barrier within HSE (27 meV) is larger than with PBE (11 meV), but still small. These data suggest that quantitative results require the use of HSE. AIMD calculations based on the PBE functional are expected, however, to capture the essential physics of the DB assisted exciton transfer, while transition probabilities and transition times will be affected by the functional. This does not hold for the approximation used to model the dispersion interactions: Test calculations for the Tc/Si

TABLE I. Si and Tc excitation energies (in eV) calculated within constrained DFT using different functionals in comparison to experimental data from Refs. [47][a] [48][b], and [49][c]. Here $E^{*(T_1)}$ and E^{Δ} denote T_1 triplet exciton energy and band gap or HOMO-LUMO separation, respectively.

	HSE	PBE	HSE40	B3LYP	Exp.
$E^{\Delta}_{\text{Si bulk}}$	1.21	0.57	1.64	1.99	1.13[a]
$E^{\Delta}_{\text{Tc molecule}}$	4.68	4.54	4.74	4.69	5.9[b]
$E^{*(T_1)}_{\text{Tc bulk}}$	1.26	1.24	1.27	1.30	1.25[c]

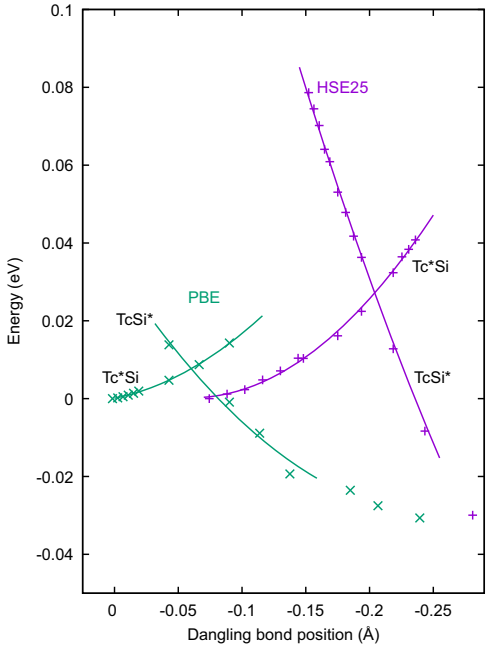

FIG. 7. Energetics of exciton transfer from the Tc layer (HD model) into the defective Si(111):H substrate calculated within PBE and HSE. The PES are calculated starting from the lowest energy configuration of Tc- and Si-localized triplet excitons, i.e., Tc*Si and TcSi*, respectively (see Ref. [35] for atomic coordinates). The interface structures are subsequently fully relaxed for various vertical Si DB atom positions, that serve as reaction coordinate. Solid lines are to guide the eye.

(001):H high-density and low-density interfaces using the PBE + D3 approach [46] yield essentially identical atomic structures and electronic states in the band gap region than obtained with PBE + D2.

The electronic wave functions are expanded into plane waves up to an energy cutoff of 30 Ry. This cutoff provides converged results as verified by expanding the cutoff to 60 Ry. The interface Brillouin zone is sampled using a $2 \times 2 \times 1$ mesh for structural relaxation and AIMD calculations. The electronic density of states is calculated using a $4 \times 4 \times 1$ grid. Energy and force convergence criteria are 10^{-8} Ry and 10^{-4} Ry$/a_B$, respectively. The Verlet algorithm with a time step of 1 fs is used for the AIMD.

The atomic structures of the AIMD starting configurations are obtained by slightly randomizing and subsequently thermalizing (for 400 fs) the snapshots (50 fs apart) of a ground-state molecular dynamics trajectory. The electronic starting configuration is then prepared by occupying the electronic states such as to model the lowest Tc spin triplet. The total magnetization of the system is conserved throughout the AIMD simulation for the sake of numerical stabilization. The nonadabatic coupling coefficients used to obtain the hopping probabilities between the PES are calculated by using modules from the Libra-X package [32].

[1] R. E. Blankenship, *Molecular Mechanisms of Photosynthesis* (Wiley-Blackwell, Hoboken, NJ, 2021).
[2] Y. Sun, N. C. Giebink, H. Kanno, B. Ma, M. E. Thompson, and S. R. Forrest, Nature (London) **440**, 908 (2006).
[3] P. Peumans, A. Yakimov, and S. R. Forrest, J. Appl. Phys. **93**, 3693 (2003).
[4] A. Holzhey, C. Uhrich, E. Brier, E. Reinhold, P. Bäuerle, K. Leo, and M. Hoffmann, J. Appl. Phys. **104**, 064510 (2008).
[5] A. Ullah and P. Dral, Nat. Commun. **13**, 1930 (2022).
[6] M. Cainelli and Y. Tanimura, J. Chem. Phys. **154**, 034107 (2021).
[7] S. M. Falke, C. A. Rozzi, D. Brida, M. Maiuri, M. Amato, E. Sommer, A. D. Sio, A. Rubio, G. Cerullo, E. Molinari, and C. Lienau, Science **344**, 1001 (2014).
[8] C. Schwermann and N. Doltsinis, Phys. Chem. Chem. Phys. **22**, 10526 (2020).
[9] L. Schmidt-Mende, S. Kraner, and A. Fakharuddin, *Organic and Hybrid Solar Cells* (De Gruyter, Berlin, 2022).
[10] M. Einzinger, T. Wu, J. Kompalla, H. Smith, C. Perkinson, L. Nienhaus, S. Wieghold, D. Congreve, A. Kahn, M. Bawendi, and M. Baldo, Nature (London) **571**, 90 (2019).
[11] B. Daiber, S. Maiti, S. M. Ferro, J. Bodin, A. F. J. van den Boom, S. L. Luxembourg, S. Kinge, S. P. Pujari, H. Zuilhof, L. D. A. Siebbeles, and B. Ehrler, J. Phys. Chem. Lett. **11**, 8703 (2020).
[12] R. W. MacQueen, M. Liebhaber, J. Niederhausen, M. Mews, C. Gersmann, S. Jäckle, K. Jäger, M. J. Y. Tayebjee, T. W. Schmidt, B. Rech, and K. Lips, Mater. Horiz. **5**, 1065 (2018).
[13] G. B. Piland, J. J. Burdett, T.-Y. Hung, P.-H. Chen, C.-F. Lin, T.-L. Chiu, J.-H. Lee, and C. J. Bardeen, Chem. Phys. Lett. **601**, 33 (2014).
[14] B. Ehrler, B. J. Walker, M. L. Böhm, M. W. Wilson, Y. Vaynzof, R. H. Friend, and N. C. Greenham, Nat. Commun. **3**, 1019 (2012).
[15] D. N. Congreve, J. Lee, N. J. Thompson, E. Hontz, S. R. Yost, P. D. Reusswig, M. E. Bahlke, S. Reineke, T. V. Voorhis, and M. A. Baldo, Science **340**, 334 (2013).
[16] W. Shockley and H. J. Queisser, J. Appl. Phys. **32**, 510 (2004).
[17] A. Rao and R. Friend, Nat. Rev. Mater. **2**, 17063 (2017).
[18] J. M. Luther and J. C. Johnson, Nature (London) **571**, 38 (2019).
[19] A. F. J. van den Boom, S. Ferro, M. Gelvez-Rueda, H. Zuilhof, and B. Ehrler, J. Phys. Chem. Lett. **14**, 4454 (2023).
[20] D. C. Moritz, W. Calvet, M. A. Zare Pour, A. Paszuk, T. Mayer, T. Hannappel, J. P. Hofmann, and W. Jaegermann, Solar RRL **7**, 2201063 (2023).
[21] P. Giannozzi *et al.*, J. Phys. Condens. Matter **21**, 395502 (2009).
[22] P. Giannozzi *et al.*, J. Phys. Condens. Matter **29**, 465901 (2017).
[23] J. P. Perdew, K. Burke, and M. Ernzerhof, Phys. Rev. Lett. **77**, 3865 (1996).
[24] S. Grimme, J. Comput. Chem. **27**, 1787 (2006).
[25] J. Heyd, G. E. Scuseria, and M. Ernzerhof, J. Chem. Phys. **118**, 8207 (2003).
[26] B. Kaduk, T. Kowalczyk, and T. Van Voorhis, Chem. Rev. **112**, 321 (2012).
[27] O. Pankratov and M. Scheffler, Phys. Rev. Lett. **75**, 701 (1995).
[28] E. Artacho, M. Rohlfing, M. Côté, P. D. Haynes, R. J. Needs, and C. Molteni, Phys. Rev. Lett. **93**, 116401 (2004).
[29] M. L. Tiago, S. Ismail-Beigi, and S. G. Louie, J. Chem. Phys. **122**, 094311 (2005).
[30] T. Frigge, B. Hafke, T. Witte, B. Krenzer, C. Streubuhr, A. S. Syed, V. M. Trontl, I. Avigo, P. Zhou, M. Ligges, D. von der Linde, U. Bovensiepen, M. H. von Hoegen, S. Wippermann, A. Lücke, S. Sanna, U. Gerstmann, and W. G. Schmidt, Nature (London) **544**, 207 (2017).
[31] C. W. Nicholson, A. Lücke, W. G. Schmidt, M. Puppin, L. Rettig, R. Ernstorfer, and M. Wolf, Science **362**, 821 (2018).
[32] E. Pradhan, K. Sato, and A. V. Akimov, J. Phys. Condens. Matter **30**, 484002 (2018).
[33] H. J. C. Berendsen, J. P. M. Postma, W. F. van Gunsteren, A. DiNola, and J. R. Haak, J. Chem. Phys. **81**, 3684 (1984).
[34] J. Niederhausen, R. W. MacQueen, K. Lips, H. Aldahhak, W. G. Schmidt, and U. Gerstmann, Langmuir **36**, 9099 (2020).
[35] See Supplemental Material at http://link.aps.org/supplemental/10.1103/PhysRevLett.132.076201 for atomic coordinates.
[36] S. M. Janke, M. Rossi, S. V. Levchenko, S. Kokott, M. Scheffler, and V. Blum, Electron. Struct. **2**, 035002 (2020).
[37] D. C. Moritz, I. A. Ruiz Alvarado, M. A. Zare Pour, A. Paszuk, T. Frieß, E. Runge, J. P. Hofmann, T. Hannappel, W. G. Schmidt, and W. Jaegermann, ACS Appl. Mater. Interfaces **14**, 47255 (2022).

[38] M. Stutzmann and D. K. Biegelsen, Phys. Rev. B **40**, 9834 (1989).
[39] O. Astakhov, R. Carius, Y. Petrusenko, V. Borysenko, D. Barankov, and F. Finger, J. Phys. Condens. Matter **24**, 305801 (2012).
[40] M. Rohrmüller, W. G. Schmidt, and U. Gerstmann, Phys. Rev. B **95**, 125310 (2017).
[41] B. M. George, J. Behrends, A. Schnegg, T. F. Schulze, M. Fehr, L. Korte, B. Rech, K. Lips, M. Rohrmüller, E. Rauls, W. G. Schmidt, and U. Gerstmann, Phys. Rev. Lett. **110**, 136803 (2013).
[42] C. Braun, S. Neufeld, U. Gerstmann, S. Sanna, J. Plaickner, E. Speiser, N. Esser, and W. G. Schmidt, Phys. Rev. Lett. **124**, 146802 (2020).
[43] D. L. Staebler and C. R. Wronski, Appl. Phys. Lett. **31**, 292 (1977).
[44] A. Kołodziej, Opto-Electron. Rev. **12**, 21 (2004), https://optor.wat.edu.pl/abstract12_1.htm#21.
[45] A. D. Becke, J. Chem. Phys. **98**, 5648 (1993).
[46] S. Grimme, J. Antony, S. Ehrlich, and H. Krieg, J. Chem. Phys. **132**, 154104 (2010).
[47] O. Madelung, W. von der Osten, and U. Rössler, *Intrinsic Properties of Group IV Elements and III-V, II-VI and I-VII Compounds*, edited by O. Madelung (Springer-Verlag, Berlin, 1987).
[48] *NIST Chemistry WebBook*, edited by P. Linstrom and W. Mallard (National Institute of Standards and Technology, Gaithersburg MD, 20899, 2023), https://webbook.nist.gov/chemistry/.
[49] Y. Tomkiewicz, R. P. Groff, and P. Avakian, J. Chem. Phys. **54**, 4504 (1971).